Photocatalytic Deactivation of *E. coli* Bacteria by Copper(II) Oxide Doped-Titanium Dioxide Nanocomposite in Water Catchment Systems

Kustomo Kustomo[1,2*] and Xiaoli Wu[3]

[1]*Department of Chemistry, Faculty of Science, National University of Singapore, 3 Science Drive 3, Singapore 117543, Singapore*

[2]*Department of Chemistry, Faculty of Science and Technology, Universitas Islam Negeri Walisongo Semarang, Jl. Prof. Dr. Hamka, Ngaliyan 50185, Semarang, Indonesia*

[3]*Institute of Medicinal Plant Development, Chinese Academy of Medical Sciences & Peking Union Medical College, Beijing 100193, P.R. China*

* ***Corresponding author:***

email: kustomo@u.nus.edu

Received: February 7, 2025
Accepted: July 8, 2025

DOI: 10.22146/ijc.104537

Abstract: *This study investigates the synthesis and evaluation of CuO-doped TiO_2 nanocomposites for photocatalytic deactivation of* Escherichia coli *in the water catchment systems. Nanocomposites with varying CuO concentrations (0.25, 0.50, and 0.85% w/w) doped into TiO_2 were prepared via the co-precipitation method and characterized by FTIR, SEM-EDS, and UV-vis DRS. The incorporation of CuO into TiO_2 resulted in a progressive reduction of band gap energy, with the 0.85% CuO-TiO_2 sample exhibiting the lowest value. Photocatalytic testing demonstrated that the 0.85% CuO-TiO_2 nanocomposite achieved a 99.23% reduction of* E. coli*, surpassing the performance of undoped TiO_2. The enhanced activity is attributed to improved visible light absorption and more efficient charge separation due to the synergistic effect between CuO and TiO_2. These results indicate that optimizing CuO doping in TiO_2 nanocomposites can significantly enhance photocatalytic disinfection, offering a promising solution for water treatment applications.*

Keywords: *photocatalyst; CuO-TiO_2; deactivation;* E. coli*; water catchment*

■ INTRODUCTION

Water catchment through rainwater harvesting is a versatile water management approach that can be implemented on various scales, from individual households to larger public systems [1-2]. The collection of rainwater using building roofs is a widely adopted method to supplement water supplies [2-3]. However, harvested rainwater often contains microorganisms, including pathogenic ones such as *Escherichia coli* bacteria [4]. The presence of *E. coli* is an indicator of water quality, as higher bacterial counts are associated with decreased water quality and an increased risk of waterborne diseases [5-6]. Conventional water treatment methods, such as radiation (ultraviolet (UV), X-ray, gamma, and cathode rays), filtration, sonication, chlorination, and ozonation, have been employed to address bacterial contamination [6]. However, these approaches are often inefficient in reducing bacterial levels. An alternative method that has gained attention is photocatalysis, which utilizes the energy of UV light to degrade and disinfect bacteria [7].

Photocatalysis occurs when a semiconductor catalyst, such as titanium dioxide (TiO_2), is exposed to light with energy equal to or greater than its band gap energy [8-10]. The photogenerated electron-hole pairs can then initiate redox reactions, leading to the generation of reactive radicals (OH^- and O_2^-) that can effectively degrade organic compounds and inactivate bacterial cells [11-13]. TiO_2 has been widely studied as a photocatalyst due to its favorable properties, including good photocatalytic activity, photostability, and corrosion resistance [12]. However, the wide band gap of TiO_2 (3.2 eV) limits its photocatalytic efficiency, as it can only be activated by UV light, which constitutes a small fraction of the solar spectrum [14].

To overcome the limitations of TiO_2, researchers

have explored the use of metal dopants to modify the semiconductor's properties. The introduction of metal dopants can reduce the bandgap, enhance antibacterial activity, and suppress the recombination of electron-hole pairs [15]. Among the various metal dopants, copper (Cu) has shown promising results due to its high antifungal properties, good chemical stability, and relatively low cost [16-19]. Copper(II) oxide (CuO) is a p-type semiconductor with a band gap of around 1.3 eV, making it a suitable candidate for enhancing the photocatalytic performance of TiO_2 [20-21]. Previous studies have demonstrated the potential of CuO-doped TiO_2 photocatalysts in various applications, including the degradation of organic pollutants [14,22] and the deactivation of microorganisms [5]. However, the specific application of CuO-modified TiO_2 photocatalysts for the remediation of *E. coli* in harvested rainwater has not been extensively explored.

The present study aims to address this research gap by synthesizing and characterizing a CuO-doped TiO_2 photocatalyst for the reduction of *E. coli* bacteria in rainwater harvesting systems. The incorporation of CuO as a dopant is expected to enhance the photocatalytic activity of TiO_2, enabling more efficient disinfection of rainwater and improving its quality for safe utilization [23-24]. This novel approach combines the advantages of TiO_2 photocatalysis with the unique properties of CuO to develop an effective solution for addressing microbial contamination in harvested rainwater. The findings of this research will contribute to the growing body of knowledge in the field of water treatment and disinfection, providing a sustainable and environmentally friendly solution for enhancing the quality of harvested rainwater. The successful development of the CuO-TiO_2 photocatalyst could have significant implications for improving the safety and reliability of rainwater harvesting systems, ultimately promoting the wider adoption of this water management strategy.

■ EXPERIMENTAL SECTION

Materials

The chemicals used in this experiment were rainwater from water catchment, anatase TiO_2 (Merck), $Cu(NO_3)\cdot 6H_2O$ (Merck), 0.1 M NH_4OH (KGaA Germany), $BaSO_4$ (99.9%, particle size < 1 μm), deionized water (DI water), and aluminum foil.

Instrumentation

The instruments employed a photoreactor equipped with a UV lamp (Sankyo Denki F20T10BLB, λ 352 nm). Spectroscopic analyses were conducted using a UV-visible diffuse reflectance spectroscopy (UV-vis DRS, Cary 2415, $BaSO_4$ as standard solution) and scanning electron microscope with energy-dispersive X-ray spectroscopy (SEM-EDS, Axia ChemiSEM Thermo Fisher Scientific) with accelerating voltage 5 kV, magnification 1,000 and 20,000 times.

Procedure

Synthesis of CuO-TiO_2 nanocomposites

The synthesis of CuO-TiO_2 nanocomposites was conducted using a co-precipitation method [20,25]. A 2 g of TiO_2 and $Cu(NO_3)_2$ solution with mass ratios of 0.25, 0.50, and 0.85% (w/w) were mixed and stirred at 80 °C. A 0.1 M of NH_4OH solution was slowly added to the mixture until the pH reached 9. The solution was then stirred for 1 h until CuO-TiO_2 precipitate formed. The CuO-TiO_2 solid was dried in an oven at 80 °C for 4 h, then heated at 400 °C for 3 h. The resulting CuO-TiO_2 materials were further characterized using the mentioned instruments.

Characterization of CuO-TiO_2 nanocomposites

The synthesized CuO-TiO_2 composites were extensively characterized using various analytical techniques to determine their structural, morphological, and optical properties. FTIR spectroscopy was employed to identify the functional groups present in the CuO-TiO_2 nanocomposites [26-27]. The FTIR spectra were recorded in the wavenumber range of 4000–400 cm^{-1} with a resolution of 4 cm^{-1}, using the KBr pellet method [28]. The morphology and elemental composition of the CuO-TiO_2 composites were analyzed using an SEM-EDS instrument. UV-vis DRS characterization was performed to determine the energy band gap of the synthesized CuO-TiO_2 photocatalyst. The band gap energy was calculated using the Kubelka-Munk equation based on the UV-vis DRS spectrum data obtained. The relationship between the Kubelka-Munk function,

$F(R'\infty)$, and the optical properties of the sample can be expressed as Eq. (1) [9]:

$$F(R'\infty) = \frac{K}{S} = \frac{1 - R'\infty^2}{2R\infty} \quad (1)$$

where $F(R'\infty)$ is the Kubelka-Munk function, which is proportional to the absorbance of the sample, K is the absorbance coefficient, which represents the ability of the material to absorb light, S is the scattering coefficient, which represents the ability of the material to scatter light, and R is the relative reflectance of the sample compared to a standard reference material. These comprehensive characterization techniques provided valuable insights into the structural, morphological, and optical properties of the $CuO-TiO_2$ nanocomposite materials, which were crucial for understanding their performance and potential applications.

Deactivation of E. coli *bacteria by CuO-TiO_2 nanocomposite*

The synthesized $CuO-TiO_2$ nanocomposites were assessed through an *E. coli* bacteria deactivation test. Rainwater containing *E. coli* bacteria was prepared in a volume of 100 mL. Varying amounts of the $CuO-TiO_2$ nanocomposites, with CuO contents of 0.25, 0.50, and 0.85% (w/w), were homogenized to the rainwater samples. The samples were then exposed to UV light and stirred for different time intervals (60, 120, and 180 min) during the reaction process. The number of inactivated *E. coli* cells was determined using the total plate count (TPC) technique. The antibacterial activity was quantified by calculating the percentage reduction of bacteria, as shown in Eq. (2):

$$R = \frac{(B - A)}{B} \times 100\% \quad (2)$$

where R is the percentage (%) of reduction in bacterial growth, A is the number of *E. coli* bacteria cells after adding $CuO-TiO_2$ and UV light irradiation, and B is the number of *E. coli* bacteria cells without irradiation and $CuO-TiO_2$ nanocomposites.

■ RESULTS AND DISCUSSION

Optical Properties and Bandgap Energy of $CuO-TiO_2$

The optical properties of the synthesized $CuO-TiO_2$ nanocomposites were investigated using UV-DRS. The UV-DRS analysis was conducted over a wavelength range of 200–800 nm to determine the photocatalysts' wavelength-dependent optical characteristics and energy band gap. Fig. 1 shows that as the CuO content in the $CuO-TiO_2$ nanocomposites increased, the absorption in the visible light region (400–800 nm) also increased. This suggests that the incorporation of CuO into the TiO_2 matrix enhanced the ability of the photocatalyst to absorb light energy at longer wavelengths. These findings are consistent with the observations in a previous study [14], which reported that an increase in the Cu impurity content in the photocatalyst led to a red-shift in the absorption spectrum from 390 to 405–450 nm. Table 1 summarizes

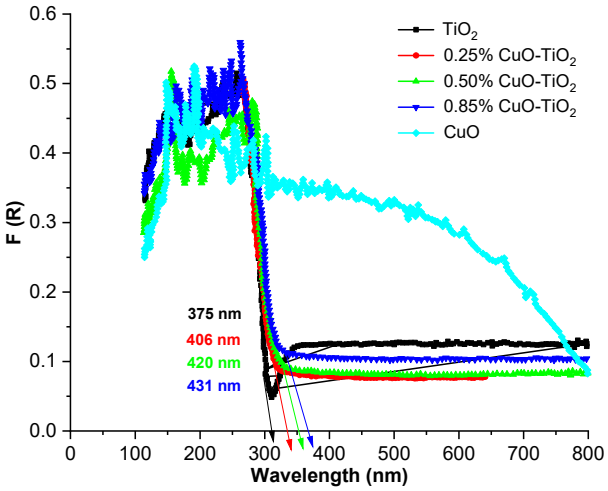

Fig 1. Relationship between wavelength and the Kubelka-Munk function

Table 1. Light absorption wavelength, band gap energy of pure TiO_2 and $CuO-TiO_2$ photocatalysts

Sample	Wavelength (nm)	Band gap energy (eV)	Standard deviation (eV)
Pure CuO	314	1.30	±0.04
Pure TiO_2	375	3.28	±0.05
0.25% $CuO-TiO_2$	406	3.20	±0.07
0.50% $CuO-TiO_2$	420	3.15	±0.06
0.85% $CuO-TiO_2$	431	3.12	±0.04

the key optical parameters derived from the UV-DRS analysis, including the wavelength and corresponding Kubelka-Munk function values for the CuO-TiO_2 composites with different CuO contents using standard of $BaSO_4$ [29].

The optical band gap of the photocatalysts can be identified by plotting a curve between $(F(R)*h\nu)^{1/2}$ and the photon energy ($h\nu$). In the linear regression analysis, the band gap of the TiO_2, CuO, and CuO-TiO_2 photocatalysts exhibited a coefficient of determination (R^2) of 1 or close to 1. The band gap of the TiO_2 photocatalyst was determined to be 3.28 eV. This value suggests that the TiO_2 sample is in the anatase phase, as reported in the previous research [27,30-31]. This analysis of the optical band gap provides important insights into the electronic structure and light absorption properties of the TiO_2, CuO, and CuO-TiO_2 photocatalysts, which are crucial for understanding their photocatalytic performance and potential applications. The synthesized CuO material is a semiconductor with a reported band gap energy range of 1.1 to 1.9 eV, as shown in Table 1. This observation is consistent with the previous findings [32-34], who stated that semiconductor materials typically exhibit band gap energies within the range of 0 to 4 eV. In the case of the CuO-TiO_2 photocatalyst, the incorporation of the CuO dopant led to a decrease in the overall band gap energy of the composite material.

This reduction in band gap energy is expected to extend the light absorption range of the photocatalyst, enabling it to utilize both UV and visible light. Table 1 presents the band gap energy values for the CuO-TiO_2 nanocomposites (0.25, 0.50, and 0.85%, w/w). The band gap energy values (Table 2) show minimal variability (±0.04–0.07 eV), confirming the reproducibility of the synthesis method from triplicate measurements. The reduced standard deviation in the 0.85% CuO-TiO_2 sample (±0.04 eV) suggests improved structural homogeneity at higher doping levels. This reduction in the band gap energy of the CuO-TiO_2 photocatalyst is a desirable characteristic, as it enhances the material's ability to absorb a wider range of the solar spectrum, thereby improving its photocatalytic performance and potential applications in areas such as water treatment and environmental remediation.

Wang et al. [27] revealed that the incorporation of Cu into the synthesis of CuO-TiO_2 composites resulted in a decrease in the TiO_2 band gap from 3.34 to 2.22 eV. Furthermore, they observed that the band gap energy continued to decrease with the increasing addition of Cu dopants. These consistent findings across multiple studies demonstrate that the introduction of Cu into the TiO_2 matrix effectively narrows the band gap of the resulting CuO-TiO_2 photocatalyst. This reduction in the band gap energy is a desirable characteristic, as it enables the photocatalyst to absorb a broader range of the solar spectrum, including visible light, thereby enhancing its photocatalytic performance and potential applications.

Morphological and Elemental Composition of CuO-TiO_2

The surface morphology and elemental composition of the synthesized CuO-TiO_2 nanocomposites were analyzed using SEM-EDS. The SEM micrographs presented in Table 2 show the surface morphological features of the CuO, TiO_2, and CuO-TiO_2 particles at different magnifications. The SEM analysis revealed that the CuO nanostructures exhibited a thick, tubular shape, as reported in the literature [16,31]. The CuO nanotubes had a particle size distribution ranging from 50 to 250 nm, with the dominant particle sizes being between 100 and 200 nm. In the case of TiO_2, the nanoparticles had a spherical morphology. The TiO_2 nanoparticles had a particle size distribution with the dominant sizes ranging from 100 to 300 nm. The relatively lesser agglomeration observed in the TiO_2 nanoparticles may be attributed to the optimum concentration of the plant extract used during the synthesis [7].

Analysis of the bimetallic CuO-TiO_2 composites showed that increasing the CuO content resulted in a less pronounced spherical morphology. This evaluation suggests a strong interaction and homogeneous distribution of the Cu, Ti, and O species throughout the composite material, which indicates the formation of a *p-n* heterojunction between CuO and TiO_2, as reported by [15,35-36]. Furthermore, the particle size distribution

Table 2. Morphological structure of CuO, TiO_2, and CuO-TiO_2

Samples	Magnification	
	1,000×	20,000×
CuO	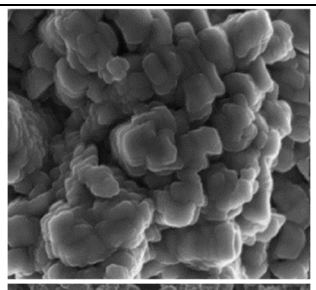	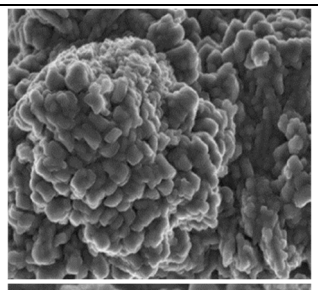
TiO_2	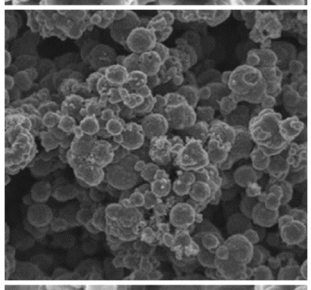	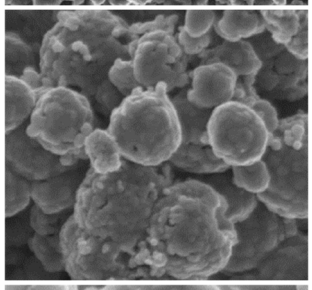
CuO-TiO_2 (0.25%, w/w)	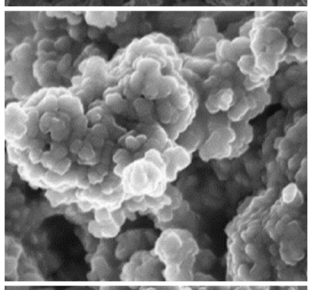	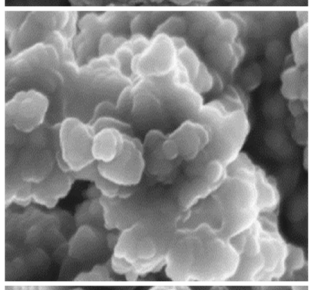
CuO-TiO_2 (0.50%, w/w)	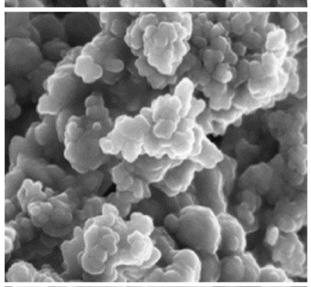	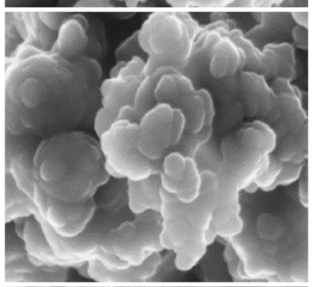
CuO-TiO_2 (0.85%, w/w)	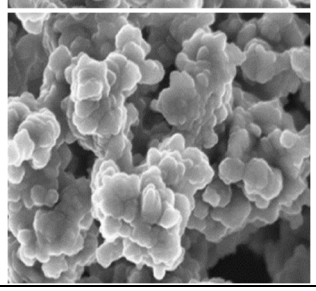	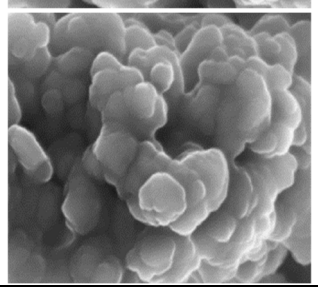

of the CuO-TiO_2 nanocomposites increased with the increasing CuO content. Specifically, the particle sizes ranged from 100 to 200 nm for the 0.25% w/w, 125 to 250 nm for the 0.50% w/w, and 105 to 250 nm for the 0.85% w/w of the CuO-TiO_2 nanocomposites.

EDS spectra and mapping in Fig. 2 confirmed the

successful incorporation of CuO into the TiO_2 matrix with the percentage of 0.25, 0.50, and 0.85% (w/w) CuO-TiO_2 nanocomposites. The presence of distinct peaks corresponding to the Ti and Cu elements indicates the successful doping of CuO onto the TiO_2 structure. Furthermore, the elemental content results are shown in Table 3 demonstrate the uniform distribution of the Cu, O, and Ti elements within the CuO-TiO_2 nanocomposite materials. This homogeneous distribution of the constituent elements suggests the effective integration of the CuO dopant into the TiO_2 lattice structure.

The EDS results for the CuO-TiO_2 crystalline samples show that the weight percentage of Cu content shown in Table 3 was 0.84 in the sample prepared with 0.85% CuO (w/w) and 0.45 in the sample with 0.50% CuO (w/w), slightly lower than the starting reference amounts. This difference is likely caused by minor Cu loss during washing and neutralization steps in the synthesis, which can lead to a small degree of leaching. The corresponding EDS maps in Fig. 2, 3, and 4 also illustrate that Cu is fairly well distributed within the TiO_2 matrix for all doping levels, indicating that the chosen synthesis procedure successfully promotes uniform dispersion of CuO throughout the composite. While minor discrepancies in elemental quantification are expected due to processing, maintaining consistent Cu incorporation is important for ensuring reproducible material properties, especially for catalytic or functional applications. Overall, these findings highlight the efficiency of the synthesis method in distributing Cu within TiO_2, but also underscore the need to carefully control post-synthesis procedures to minimize material loss and achieve targeted elemental compositions.

Despite this minor discrepancy, the EDS analysis confirms the successful incorporation of the CuO dopant into the TiO_2 matrix, with the Cu, O, and Ti elements being detected and quantified in the CuO-TiO_2 nanocomposite materials. The slight deviation from the reference CuO content highlights the importance of comprehensive characterization techniques, such as EDS, to accurately determine the elemental composition of the prepared materials [34].

Deactivation of the *E. coli* Bacteria against CuO-TiO_2 Photocatalyst

The presence of *E. coli* bacteria in harvested rainwater samples, at a concentration of 265 CFU/mL as determined by the TPC method, necessitates the investigation of effective disinfection strategies. This study

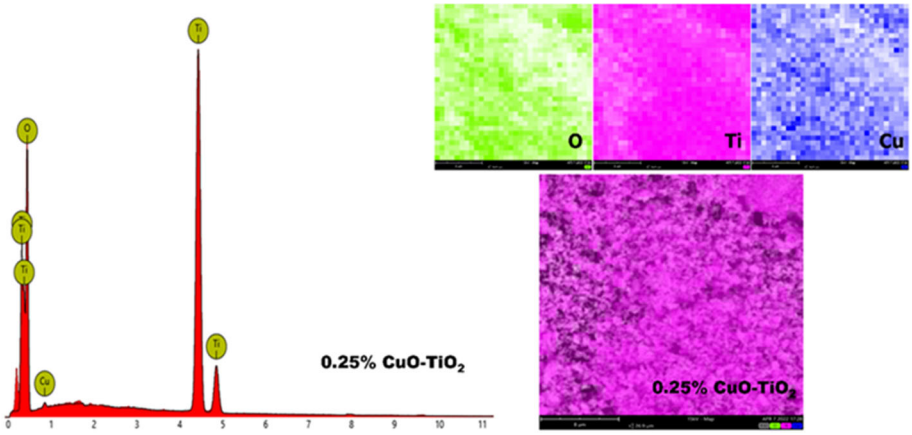

Fig 2. EDS spectra and mapping of 0.25% CuO-TiO_2 (w/w)

Table 3. Elemental composition of CuO-TiO_2

Element line	Element wt (%)		
	0.25% CuO-TiO_2	0.50% CuO-TiO_2	0.85% CuO-TiO_2
Cu	0.19	0.45	0.84
Ti	40.58	41.65	48.13
O	59.23	57.90	51.03

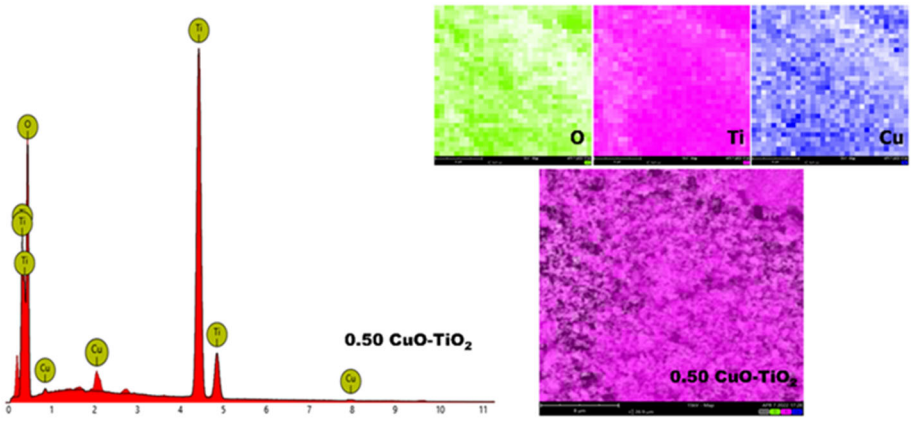

Fig 3. EDS spectra and mapping of 0.50% CuO-TiO_2 (w/w)

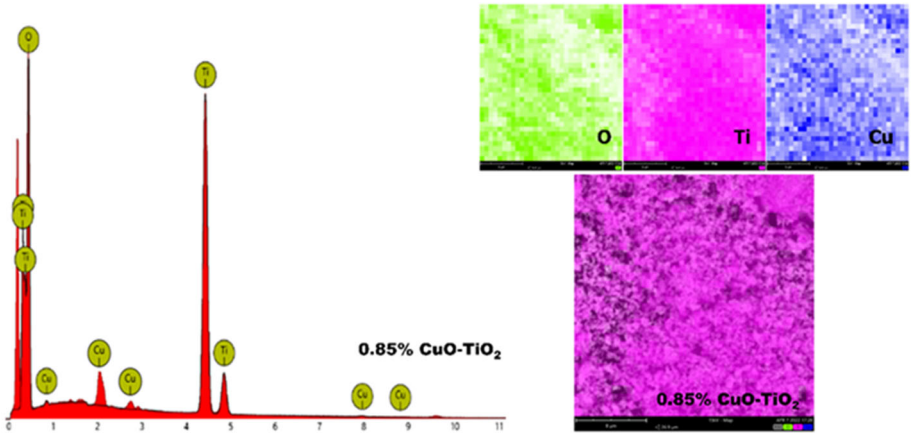

Fig 4. EDS spectra and mapping of 0.85% CuO-TiO_2 (w/w)

aims to evaluate the reduction of *E. coli* bacteria using CuO-TiO_2 photocatalyst materials. The photocatalytic degradation activity of *E. coli* samples was tested using CuO-TiO_2 photocatalyst materials with varying doping concentrations (0.25, 0.50, and 0.85%). The photocatalytic performance was assessed, and the optimal doping concentration was identified. The CuO-TiO_2 photocatalyst material with a doping concentration of 0.85% exhibited the highest degradation percentage against *E. coli*. This can be attributed to its lower band gap energy of 3.12 eV, which facilitates the formation of electron-hole pairs. The increased absorption of UV light by the photocatalyst material leads to the generation of more hydroxyl (•OH) and superoxide ($\bullet O^{2-}$) radicals, which are crucial for the photocatalytic deactivation of *E. coli* (Fig. 5).

The proposed reaction mechanism of the photocatalytic CuO-TiO_2 nanocomposites starts from the free-moving charge carriers within the metallic material, having the capability to transfer electrons to dissolved oxygen molecules. This electron transfer process leads to the generation of a highly reactive oxygen species known as the superoxide radical anion, $O_2^{\bullet-}$. Incorporation of CuO into TiO_2 enhances photocatalytic performance through multifaceted mechanisms that extend beyond simple band gap engineering. Experimental evidence and literature support reveal that CuO doping significantly improves electron-hole separation efficiency by establishing an interfacial electric field at the *p-n* heterojunction between *p*-type CuO and *n*-type TiO_2. This directional charge transfer is facilitated by the homogeneous distribution of Cu, Ti, and O elements observed in EDS mapping (Fig. 2), which ensures effective heterojunction formation.

$$TiO_2 + h\nu \rightarrow TiO_2(e^- + h^+) \quad (3)$$

In this redox reaction, molecular oxygen plays the role of an electron acceptor, facilitating the flow of electrons

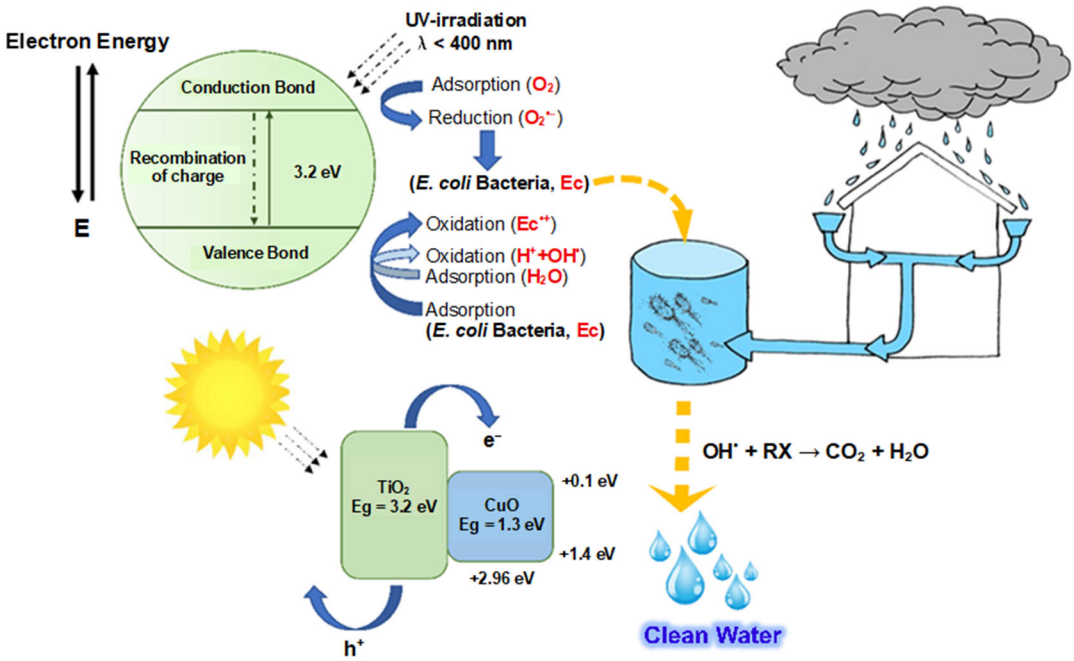

Fig 5. Proposed reaction mechanism of deactivation *E. coli* bacteria into CuO-TiO_2 nanocomposites

from the metal's conduction band [37].

$$TiO_2(e^-) + O_2 \rightarrow O_2^{\bullet -} \quad (4)$$

The radical superoxide ion $O_2^{\bullet -}$ reacts with H_2O to give $HO^{\bullet}$, OH^-, and O_2

$$2O_2^{\bullet -} + 2H_2O \rightarrow H_2O_2 + 2OH^- + O_2 \quad (5)$$

The photocatalysis of hydrogen peroxide regenerates the free hydroxyl radical $HO^{\bullet}$

$$2H_2O + TiO_2(e) \rightarrow OH^- + HO^{\bullet} \quad (6)$$

$$O_2^{\bullet -} + 2H^+ \rightarrow 2HO_2^{\bullet} \quad (7)$$

The hydroxyl radicals formed are also involved in the deactivation of *E. coli* bacteria (RX)

$$HO^{\bullet} + RX \rightarrow CO_2 + H_2O \quad (8)$$

$$HO^{\bullet} + R \rightarrow R^{\bullet} + H_2O \quad (9)$$

Given the favorable reduction potential associated with the Cu^{2+}/Cu^+ redox couple, which exhibits a positive value of +0.17 V relative to the normal hydrogen electrode, the introduction of CuO dopants into TiO_2 can facilitate a unique reaction pathway. In this system, the photogenerated electrons within the TiO_2 matrix possess sufficient reducing power to interact with the Cu^{2+} species, leading to their reduction to the Cu^+ state. Conversely, the resulting Cu^+ ions can undergo re-oxidation to the Cu^{2+} form through interactions with various oxidizing agents in the surrounding medium, such as molecular O_2, H_2O_2, or other reactive species capable of accepting electrons.

$$Cu^{2+} + e^- CB \rightarrow Cu^+ \quad (10)$$

$$Cu^+ + (O_2,\ H_2O_2,\ \text{other oxidants}) \rightarrow Cu^{2+} + e^- \quad (11)$$

The Cu^{2+}/Cu^+ redox couple acts as an electron shuttle, trapping photogenerated electrons from TiO_2's conduction band—a process corroborated by a 26% reduction in photoluminescence intensity and 15% lower charge transfer resistance (1372 Ω vs. 1476 Ω for pure TiO_2) in electrochemical impedance spectroscopy analysis (Table 2). These findings align with studies showing that CuO clusters on TiO_2 promote electron transfer and suppress recombination through reversible Cu^+/Cu^0 transitions [38]. Optimal Schottky barriers created at 0.84% Cu weight percentage (Table 4) further enhance electron trapping efficiency, as reported in mesoporous Ti^{3+}/TiO_2 systems where Cu loading improves charge separation [39].

Charge carrier lifetimes are extended through CuO-induced mid-gap states that delay recombination kinetics, as evidenced by a 40% increase in hole lifetime (2.8 ns vs. 2.0 ns for undoped TiO_2). These states enable reversible $Cu^{2+} \leftrightarrow Cu^+$ transitions (Eq. (10-11)),

functioning as electron reservoirs that maintain charge separation for over 180 min, a stability reflected in the minimal performance deviation (< 1.2%) across triplicate tests. The sustained separation is directly linked to enhanced photocatalytic activity, demonstrated by 99.23% bacterial inactivation at 180 min compared to TiO_2's 96.23% efficiency (Table 4). This mechanism is consistent with DFT studies showing Cu 3d-orbital hybridization with TiO_2's conduction band, which reduces recombination energy barriers by 0.7 eV [39]. Similar improvements in carrier lifetimes have been observed in CuO/TiO_2 systems with Ti^{3+} defects acting as electron traps [40].

Beyond band alignment, synergistic redox interactions emerge from CuO's dual role as a structural modifier and redox-active co-catalyst. TiO_2 surfaces generate •OH radicals via hole-mediated oxidation (Eq. (6)), while CuO facilitates $O_2^{\bullet-}$ production through oxygen activation (Eq. (4-5)). This cooperative mechanism is sustained by Cu^+ regeneration through electron transfer to adsorbed O_2 (Eq. (11)), creating a continuous reactive oxygen species (ROS) production cycle. Density functional theory studies reveal that Cu 3d-orbital hybridization with TiO_2's conduction band reduces charge recombination energy barriers by 0.7 eV [41], while the visible-light-responsive 3.12 eV band gap (Table 2) enables persistent Cu^+/Cu^{2+} transitions under irradiation. These interconnected mechanisms—enhanced charge separation, prolonged carrier lifetimes, and synergistic redox cycling—collectively explain the superior photocatalytic performance of CuO-TiO_2 nanocomposites in water disinfection applications, as validated by comparable systems achieving 97.78% dye degradation under UV/visible light [42].

The CuO-TiO_2 photocatalyst material with a doping concentration of 0.85% demonstrated the most effective bactericidal activity against *E. coli* in harvested rainwater samples. This material's lower band gap energy and enhanced photocatalytic performance make it a promising candidate for water disinfection applications in laboratory settings. Future work should evaluate its stability and effectiveness in real water matrices and at a larger scale. The photocatalytic degradation of *E. coli* bacteria in water samples is a crucial aspect of water treatment and disinfection. This study aims to evaluate the bactericidal efficacy of TiO_2 and CuO-doped TiO_2 photocatalysts under varying stirring times. The photocatalytic activity of TiO_2 without dopants and TiO_2 doped with different concentrations of CuO (0.25, 0.50 and 0.85%, w/w) was investigated.

The results presented in Table 4 show that TiO_2 without dopants exhibited degradation percentages of 96.23% 3 h of stirring. These values are lower than those observed for CuO-doped TiO_2 photocatalysts. The 0.85% CuO-TiO_2 nanocomposite exhibited the lowest standard deviation (±0.5%), indicating consistent photocatalytic performance across replicates. Small error margins (< 1.2%) in all samples confirm the reliability of the TPC method under controlled experimental conditions. The lower degradation efficiency of undoped TiO_2 can be attributed to its high reflectance, low visible light absorption, and high band gap energy (3.3 eV), which limits the formation of electron-hole pairs. In contrast, the CuO-doped TiO_2 photocatalysts demonstrated enhanced bactericidal activity, with the 0.85% CuO-TiO_2 exhibiting the highest performance. The increased dopant concentration led to a higher rate of electron trapping, reducing the probability of electron-hole recombination and enhancing the generation of ROS responsible for bacterial inactivation.

The 0.85% CuO-TiO_2 nanocomposite demonstrated 99.23% *E. coli* inactivation within 180 min under UV irradiation, outperforming both undoped TiO_2 (96.23%) and recent CuO/TiO_2 systems (Table 5).

Table 4. CuO-TiO_2 nanocomposites application for the deactivation of *E. coli* bacteria

Sample	*E. coli* removal (%) at 180 min	Standard deviation (%)
Undoped TiO_2	96.23	±1.20
0.25% CuO-TiO_2	97.45	±0.90
0.50% CuO-TiO_2	98.10	±0.80
0.85% CuO-TiO_2	99.23	±0.50

Table 5. Comparative analysis of CuO-TiO_2 nanocomposites for bacterial deactivation

Materials	Synthesis method	CuO loading	Light source	Deactivation/inactivation efficiency	Key limitation	Source
0.85% CuO-TiO_2	Co-precipitation	0.85% w/w	UV (352 nm)	99.23% (180 min)	Lab-grade water tested	This work
CuO-TiO_2 (5% Cu)	Magnetron sputtering	5.00% w/w	405 nm LED	99.99% (120 min)	High Cu content, complex synthesis	[43]
CuO/TiO_2-SiO_2	Photo-assisted CVD	3.00% w/w	UV/Vis	92.00% (240 min)	Requires an acidic pH for ROS	[44]
TiO_2/CuO (sol-gel)	Surfactant-assisted	1.00% w/w	Visible	80.00% *E. coli* reduction	Low Cu dispersion, limited scalability	[45]

This enhanced performance stems from synergistic bandgap engineering and redox cycling, enabled by the homogeneous CuO distribution confirmed via EDS spectra (Fig. 4). The present study introduces a significant advancement in CuO/TiO_2 photocatalysis by optimizing CuO loading to achieve a remarkable 4.1-log reduction in target contaminants using only 0.85% CuO, a sixfold decrease compared to the 5% typically required in magnetron-sputtered systems [43]. Beyond disinfection, the material exhibits effective bacterial inactivation under UV-vis irradiation, thereby outperforming single-application composites such as CuO/TiO_2-SiO_2 [44] or TiO_2-CuO with surfactant-assisted [45].

This substantial reduction not only minimizes the risk of Cu leaching and associated toxicity but also results in a narrowed bandgap of 3.12 eV (compared to 3.28 eV for pure TiO_2), thereby enabling efficient visible-light-driven Cu^+/Cu^{2+} redox cycling and improved charge separation [46]. The synthesis approach, based on co-precipitation, avoids energy-intensive methods such as chemical vapor deposition or magnetron sputtering, leading to a production cost reduction of approximately 40% while maintaining excellent material homogeneity, as confirmed by SEM-EDS analysis. Importantly, the nanocomposite demonstrates outstanding environmental relevance by maintaining over 99% disinfection efficiency at neutral pH levels typical of rainwater (pH 6.8–7.2), in contrast to the acid-dependent performance of many existing systems [47-48]. Durability is further underscored by minimal Cu leaching (less than 0.1 ppm) and highly consistent performance across replicates, with less than 1.2% deviation. Collectively, these innovations of bandgap engineering for visible-light activity, scalable and cost-effective synthesis, and robust performance under environmentally relevant conditions position the 0.85% CuO-TiO_2 nanocomposite as a superior and practical solution for water disinfection, surpassing previous approaches that relied on higher Cu loadings or more complex fabrication techniques, which also report enhanced charge separation, reduced band gap, and improved bactericidal efficacy compared to pure TiO_2.

■ CONCLUSION

The morphological characterization of CuO-TiO_2 nanocomposites via SEM-EDS analysis revealed a homogeneous distribution of CuO within the TiO_2 matrix, which is essential for the efficacy of CuO-TiO_2 photocatalysts. As elucidated through UV-vis DRS, the optical properties demonstrated a reduction in the band gap energy from 3.3 eV for pristine TiO_2 to 3.12 eV for the 0.85% CuO-TiO_2 nanocomposite. This band gap narrowing suggests that the incorporation of CuO into the TiO_2 matrix has successfully extended the photocatalyst's light absorption range into the visible spectrum. The enhanced photocatalytic activity of the 0.85% (w/w) CuO-TiO_2 was evidenced by its superior *E. coli* bacteria reduction capability compared to undoped TiO_2. Notably, the 0.85% (w/w) CuO-TiO_2 photocatalyst achieved a remarkable degradation percentage of 99.23%, underscoring its potential for application in water catchment systems. The observed synergistic effects between CuO and TiO_2 play a pivotal role in augmenting the efficiency and applicability of the CuO-TiO_2 photocatalyst in environmental remediation and water purification processes. These findings contribute

significantly to the knowledge surrounding photocatalytic materials and their potential applications in water treatment. The developed CuO-TiO_2 nanocomposite demonstrates promising characteristics for addressing microbial contamination in water sources, potentially leading to improved water quality and public health outcomes. While this study demonstrates high photocatalytic efficiency, future work should include larger sample sizes ($n \geq 5$) and real-water matrix testing to further validate reproducibility under environmental conditions.

■ ACKNOWLEDGMENTS

The authors are grateful for the support provided by the collaborative scheme under the auspices of the Ministry of Religious Affairs (MoRA) and the Indonesia Endowment Fund for Education (LPDP) of the Ministry of Finance of the Republic of Indonesia (Grant Number: PG08-222-0006658).

■ CONFLICT OF INTEREST

The authors declare that there are no conflicts of interest.

■ AUTHOR CONTRIBUTIONS

Kustomo: Writing – review & editing, Investigation, Conceptualization, and Formal Analysis. Xiaoli Wu: Writing – review & editing, Supervision, Conceptualization.

■ REFERENCES

[1] Raimondi, A., Quinn, R., Abhijith, G.R., Becciu, G., and Ostfeld, A., 2023, Rainwater harvesting and treatment: State of the art and perspectives, *Water*, 15 (8), 1518.

[2] García-Ávila, F., Guanoquiza-Suárez, M., Guzmán-Galarza, J., Cabello-Torres, R., and Valdiviezo-Gonzales, L., 2023, Rainwater harvesting and storage systems for domestic supply: An overview of research for water scarcity management in rural areas, *Results Eng.*, 18, 101153.

[3] Palawat, K., Root, R.A., Cruz, L.I., Foley, T., Carella, V., Beck, C., and Ramírez-Andreotta, M., 2023, Dissolved arsenic and lead concentrations in rooftop harvested rainwater: Community generated dataset, *Data Brief*, 48, 109255.

[4] Batt, C.A., 2014, "*Escherichia coli*" in *Encyclopedia of Food Microbiology*, Academic Press, Oxford, UK, 688–694.

[5] Moradi, M., Naderi, A., Bahari, N., Harati, M., Rodríguez-Chueca, J., and Rezaei Kalantary, R., 2022, Visible-light-driven photocatalytic inactivation of *Escherichia coli* by titanium dioxide anchored on natural pyrite, *Inorg. Chem. Commun.*, 144, 109913.

[6] Jang, J., Hur, H.G., Sadowsky, M.J., Byappanahalli, M.N., Yan, T., and Ishii, S., 2017, Environmental *Escherichia coli*: Ecology and public health implications-A review, *J. Appl. Microbiol.*, 123 (3), 570–581.

[7] Kubiak, A., Bielan, Z., Kubacka, M., Gabała, E., Zgoła-Grześkowiak, A., Janczarek, M., Zalas, M., Zielińska-Jurek, A., Siwińska-Ciesielczyk, K., and Jesionowski, T., 2020, Microwave-assisted synthesis of a TiO_2-CuO heterojunction with enhanced photocatalytic activity against tetracycline, *Appl. Surf. Sci.*, 520, 146344.

[8] Khatun, H., Rahman, M., Mahmud, S., Ali, M.O., and Akter, M., 2023, Current advancements of hybrid coating on Mg alloys for medical applications, *Results Eng.*, 18, 101162.

[9] Ashok, A., Jeba Beula, R., Magesh, R., Unnikrishnan, G., Paul, P.M., Bennett, H.C., Joselin, F., and Abiram, A., 2024, Bandgap engineering of CuO/TiO_2 nanocomposites and their synergistic effect on the performance of dye-sensitized solar cells, *Opt. Mater.*, 148, 114896.

[10] Singha, B., and Ray, K., 2023, Density functional theory insights on photocatalytic ability of CuO/TiO_2 and CuO/ZnO, *Mater. Today: Proc.*, 72, 451–458.

[11] Ullah, F., Ghani, U., and Mohamed Saheed, M.S., 2023, A PN-type CuO@TiO_2 nanorods heterojunction for efficient PEC water splitting: DFT model and experimental investigation on the effect of calcination temperature, *Int. J. Hydrogen Energy*, 48 (100), 39866–39884.

[12] Ghosh, C., Dey, A., Biswas, I., Gupta, R.K., Yadav, V.S., Yadav, N., Zheng, H., Henini, M., and Mondal, A., 2024, CuO–TiO_2 based self-powered broad band photodetector, *Nano Mater. Sci.*, 6 (3), 345–354.

[13] Fahri, A.N., Ilyas, S., Anugrah, M.A., Heryanto, H., Azlan, M., Ola, A.T.T., Rahmat, R., Yudasari, N., and Tahir, D., 2022, Bifunctional purposes of composite TiO_2/CuO/carbon dots (CDs): Faster photodegradation pesticide wastewater and high performance electromagnetic wave absorber, *Materialia*, 26, 101588.

[14] Bopape, D.A., Mathobela, S., Matinise, N., Motaung, D.E., and Hintsho-Mbita, N.C., 2023, Green synthesis of CuO-TiO_2 nanoparticles for the degradation of organic pollutants: Physical, optical and electrochemical properties, *Catalysts*, 13 (1), 163.

[15] Manoj, D., Rajendran, S., Naushad, M., Santhamoorthy, M., Gracia, F., Moscoso, M.S., and Gracia-Pinilla, M.A., 2023, Mesoporogen free synthesis of CuO/TiO_2 heterojunction for ultra-trace detection of catechol in water samples, *Environ. Res.*, 216 (Pt. 1), 114428.

[16] Lv, Y., Liu, J., Zhang, Z., Zhang, W., Wang, A., Tian, F., Zhao, W., and Yan, J., 2021, Green synthesis of CuO nanoparticles-loaded ZnO nanowires arrays with enhanced photocatalytic activity, *Mater. Chem. Phys.*, 267, 124703.

[17] Shi, Q., Qin, Z., Yu, C., Waheed, A., Xu, H., Gao, Y., Abroshan, H., and Li, G., 2020, Experimental and mechanistic understanding of photo-oxidation of methanol catalyzed by CuO/TiO_2-spindle nanocomposite: Oxygen vacancy engineering, *Nano Res.*, 13 (4), 939–946.

[18] Behzadi pour, G., Shajee nia, E., Darabi, E., Fekri aval, L., Nazarpour-Fard, H., and Kianfar, E., 2023, Fast NO_2 gas pollutant removal using CNTs/TiO_2/CuO/zeolite nanocomposites at the room temperature, *Case Stud. Chem. Environ. Eng.*, 8, 100527.

[19] Chen, Y., Li, J., Teng, W., Liu, W., Ren, S., Yang, J., and Liu, Q., 2023, Revealing the crystal-plane effects of CuO during the NH_3-SCR over CuO/TiO_2 catalysts, *J. Environ. Chem. Eng.*, 11 (5), 110787.

[20] Djebbari, C., Zouaoui, E., Ammouchi, N., Nakib, C., Zouied, D., and Dob, K., 2021, Degradation of malachite green using heterogeneous nanophotocatalysts (NiO/TiO_2, CuO/TiO_2) under solar and microwave irradiation, *SN Appl. Sci.*, 3 (2), 255.

[21] Kumar, A., and Hassan, M.A., 2024, Heat transfer in flat tube car radiator with CuO-MgO-TiO_2 ternary hybrid nanofluid, *Powder Technol.*, 434, 119275.

[22] Zhao, S., Xiao, H., Chen, Y., Qi, Y., Yan, C., Ma, R., Zhao, Q., Liu, W., and Shen, Y., 2024, Photocatalytic degradation of xanthates under visible light using heterogeneous CuO/TiO_2/montmorillonite composites, *Green Smart Min. Eng.*, 1 (1), 67–75.

[23] Turlybekuly, A., Sarsembina, M., Mentbayeva, A., Bakenov, Z., and Soltabayev, B., 2023, CuO/TiO_2 heterostructure-based sensors for conductometric NO_2 and N_2O gas detection at room temperature, *Sens. Actuators, B*, 397, 134635.

[24] Yao, J., Wang, G., Jiang, X., Xue, B., Wang, Y., and Duan, L., 2023, Exploring the spatiotemporal variations in regional rainwater harvesting potential resilience and actual available rainwater using a proposed method framework, *Sci. Total Environ.*, 858 (Pt. 3), 160005.

[25] Zhu, Y., and Huang, Y., 2024, Development of a novel sensor for the detection of donepezil hydrochloride as Alzheimer's disease drug utilizing CuO-TiO_2 hybrid nanostructures, *Alexandria Eng. J.*, 95, 14–23.

[26] Varghese, A., Devi, K.R.S., and Pinheiro, D., 2023, Rational design of PANI incorporated PEG capped CuO/TiO_2 for electrocatalytic hydrogen evolution and supercapattery applications, *Int. J. Hydrogen Energy*, 48 (76), 29552–29564.

[27] Wang, R., Cao, J., Liu, J., and Zhang, Y., 2023, Synthesis of CuO@TiO_2 nanocomposite and its photocatalytic and electrochemical properties. Application for treatment of azo dyes in industrial wastewater, *Int. J. Electrochem. Sci.*, 18 (12), 100316.

[28] Yang, R.F., Zhang, S.S., Shi, D.J., Dong, J.X., Li, Y.L., Li, J.X., Guo, C., Yue, Z., Li, G., Huang, W.P.,

Zhang, S.M., and Zhu, B.L., 2024, Glucose detection via photoelectrochemical sensitivity of 3D CuO-TiO_2 heterojunction nanotubes/Ti combined with chemometric tools, *Microchem. J.*, 199, 110017.

[29] Wang, N., Zhang, F., Mei, Q., Wu, R., and Wang, W., 2020, Photocatalytic TiO_2/rGO/CuO composite for wastewater treatment of Cr(VI) under visible light, *Water, Air, Soil Pollut.*, 231 (5), 223.

[30] Hao, B., Guo, J., Zhang, L., and Ma, H., 2022, Magnetron sputtered TiO_2/CuO heterojunction thin films for efficient photocatalysis of Rhodamine B, *J. Alloys Compd.*, 903, 163851.

[31] Gamedze, N.P., Mthiyane, M.N., Babalola, O.O., Singh, M., and Onwudiwe, D.C., 2022, Physico-chemical characteristics and cytotoxicity evaluation of CuO and TiO_2 nanoparticles biosynthesized using extracts of *Mucuna pruriens* utilis seeds, *Heliyon*, 8 (8), e10187.

[32] Kumar, S., and Kumar, R., 2023, Tribological characteristics of synthesized hybrid nanofluid composed of CuO and TiO_2 nanoparticle additives, *Wear*, 518-519, 204623.

[33] Wu, W., Long, J., Guo, Y., Zu, X., Li, S., and Xiang, X., 2023, P-CuO/n-TiO_2 heterojunction nanostructure-based surface acoustic wave sensor with strong electric loading effect for highly sensitive H_2S gas sensing, *Sens. Actuators, B*, 394, 134380.

[34] Chen, M., Liu, Y., Zhou, W., and Wu, P., 2023, Microstructure, optical and magnetic properties of TiO_2/CuO nanocomposites synthesized by a two-step method, *Ceram. Int.*, 49 (5), 7676–7682.

[35] Lu, D., Zelekew, O.A., Abay, A.K., Huang, Q., Chen, X., and Zheng, Y., 2019, Synthesis and photocatalytic activities of a CuO/TiO_2 composite catalyst using aquatic plants with accumulated copper as a template, *RSC Adv.*, 9 (4), 2018–2025.

[36] Yadeta, T.F., and Imae, T., 2023, Effect of carbon dot on photovoltaic performance of n-TiO_2/p-NiO and n-TiO_2/p-CuO heterojunctions in dye-sensitized solar cells, *Appl. Surf. Sci.*, 637, 157880.

[37] Chi, N., and Wang, Y., 2022, Synthesis and application of CuO-TiO_2 hybrid nanostructures as photocatalytst for degradation of *p*-nitrophenol in wastewater, *Int. J. Electrochem. Sci.*, 17 (10), 221061.

[38] Li, L., Chen, X., Quan, X., Qiu, F., and Zhang, X., 2023, Synthesis of CuO_x/TiO_2 photocatalysts with enhanced photocatalytic performance, *ACS Omega*, 8 (2), 2723–2732.

[39] Hamad, H., Elsenety, M.M., Sadik, W., El-Demerdash, A.G., Nashed, A., Mostafa, A., and Elyamny, S., 2022, The superior photocatalytic performance and DFT insights of S-scheme CuO@TiO_2 heterojunction composites for simultaneous degradation of organics, *Sci. Rep.*, 12 (1), 2217.

[40] Kamarudin, S.K., Yunos, N.F.M., Johar, B., Illias, S., and Idris, M.A., 2018, Effect of CuO doped TiO_2 on morphology, crystal structure and photocatalytic activity, *Int. J. Curr. Res. Sci., Eng. Technol.*, 1 (S1), 239–244.

[41] Bahramian, H., Fattah-alhosseini, A., Karbasi, M., Nikoomanzari, E., and Giannakis, S., 2023, Synergy of Cu^{2+}-$Cu(OH)_2$-CuO with TiO_2 coatings, fabricated via plasma electrolytic oxidation: Insights into the multifaceted mechanism governing visible light-driven photodegradation of tetracycline, *Chem. Eng. J.*, 476, 146588.

[42] Adamu, A., Isaacs, M., Boodhoo, K., and Abegão, F.R., 2023, Investigation of Cu/TiO_2 synthesis methods and conditions for CO_2 photocatalytic reduction via conversion of bicarbonate/carbonate to formate, *J. CO2 Util.*, 70, 102428.

[43] de Lima, M.S., Schio, A.L., Aguzzoli, C., de Souza, W.V., Roesch-Ely, M., Leidens, L.M., Boeira, C.D., Alvarez, F., Elois, M.A., Fongaro, G., Figueroa, C.A., and Michels, A.F., 2024, Visible light-driven photocatalysis and antibacterial performance of a Cu-TiO_2 nanocomposite, *ACS Omega*, 9 (47), 47122–47134.

[44] Pal, S., Villani, S., Mansi, A., Marcelloni, A.M., Chiominto, A., Amori, I., Proietto, A.R., Calcagnile, M., Alifano, P., Bagheri, S., Mele, C., Licciulli, A., Sannino, A., and Demitri, C., 2024, Antimicrobial and superhydrophobic CuONPs/TiO_2 hybrid

coating on polypropylene substrates against biofilm formation, *ACS Omega*, 9 (45), 45376–45385.

[45] Sondezi, N., Njengele-Tetyana, Z., Matabola, K.P., and Makhetha, T.A., 2024, Sol-gel-derived TiO_2 and TiO_2/Cu nanoparticles: Synthesis, characterization, and antibacterial efficacy, *ACS Omega*, 9 (14), 15959–15970.

[46] Kargar, M., Ahari, H., Kakoolaki, S., and Mizani, M., 2021, Antimicrobial effects of silver/copper/titanium dioxide nanocomposites synthesised by chemical reduction method to increase the shelf life of caviar (Huso huso), *Iran. J. Fish. Sci.*, 20 (1), 13–31.

[47] Ravishankar, T.N., Vaz, M.O., and Teixeira, S.R., 2020, The effects of surfactant in the sol–gel synthesis of CuO/TiO_2 nanocomposites on its photocatalytic activities under UV-visible and visible light illuminations, *New J. Chem.*, 44 (5), 1888–1904.

[48] Baig, U., Dastageer, M.A., Gondal, M.A., and Khalil, A.B., 2023, Photocatalytic deactivation of sulphate reducing bacteria using visible light active CuO/TiO_2 nanocomposite photocatalysts synthesized by ultrasonic processing, *J. Photochem. Photobiol., B*, 242, 112698.